








MODELING MASS RELEASE FROM NANOFIBERS – THEORY AND APPLICATION

Miljan Milosevic^{1,2,3}  [0000-0003-3789-2404], Vladimir Simic^{1,2}  [0000-0001-7842-8902], Bogdan Milicevic^{1,2}  [0000-0002-0315-8263], Dušica Stojanović⁴  [0000-0001-6308-7586], Mirjana Grković⁴, Miloš Bjelović⁵  [0000-0002-3693-445X], Petar Uskoković⁴  [0000-0001-9543-1732], Milos Kojic^{2,6,*}  [0000-0003-2199-5847]

¹ Institute for Information Technologies, University of Kragujevac, Kragujevac, Serbia.
e-mail: vsimic@kg.ac.rs

² Bioengineering Research and Development Center, Kragujevac, Serbia.
e-mail: bogdan.milicevic@uni.kg.ac.rs

³ Belgrade Metropolitan University, Belgrade, Serbia.
e-mail: miljan.m@kg.ac.rs

⁴ Faculty of Technology and Metallurgy, University of Belgrade, Belgrade, Serbia.
e-mail: duca@tmf.bg.ac.rs, mirjana.grkovic@tmf.bg.ac.rs, puskokovic@tmf.bg.ac.rs

⁵ Department for Minimally Invasive Upper Digestive Surgery, Clinical Center of Serbia, Belgrade, Serbia.

⁶ Serbian Academy of Sciences and Arts, Belgrade, Serbia.
e-mail: mkojic42@gmail.com

**corresponding author*

Abstract

This study investigates the drug release performance of electrospun composite nanofiber mats, which hold significant promise as drug carriers for site-specific delivery in therapeutic applications such as cancer therapy. Predicting drug release rates from poly(D,L-lactic-co-glycolic acid) (PLGA) nanofibers produced via emulsion electrospinning is challenging due to the system's inherent complexity. To address this, two distinct implants were fabricated at the Faculty of Technology and Metallurgy, University of Belgrade: a PLGA implant and a composite scaffold consisting of a PLGA fibrous structure enclosed between two layers of poly(ϵ -caprolactone) (PCL), prepared via emulsion-based and sequential electrospinning techniques. Computational modeling was employed to evaluate the continuous drug release from these nanofibers. The study utilized the PAK software program and a CAD user interface to create nano-implant models, with post-processing by the PAK finite element (FE) solution. Two models were developed to simulate diffusive drug release from nanofibers into a three-dimensional (3D) surrounding medium: (1) a one-dimensional (1D) finite elements with axial and radial diffusion representing the fibers, and (2) a 3D continuum discretized using composite smeared finite elements (CSFEs); with coupling of these models two models. Both models account for polymer degradation and drug hydrophobicity as partitioning at the fiber/surrounding interface. Experimental drug release rates from the scaffold were compared with computational predictions from the FE models. The results demonstrate the effectiveness of the proposed models in capturing the complex dynamics of drug release, providing valuable insights into the design and optimization of electrospun nanofiber-based drug delivery systems.

This work highlights the potential of integrating experimental and computational approaches to advance the development of controlled drug release platforms for biomedical applications.

Keywords: emulsion /sequential electrospinning, diffusion, controlled drug release, three-layered scaffold; computational modeling, composite smeared finite element, one-dimensional finite elements with axial and radial diffusion

1. Introduction

Controlled drug delivery systems are pivotal in modern therapeutics, offering precise drug encapsulation, release, and enhanced therapeutic outcomes. Over the years, researchers have explored various drug delivery platforms, including electrospun nanofiber mats, which have emerged as promising carriers for site-specific drug delivery particularly in biomedical contexts involving tissue regeneration and targeted oncological treatments (Park et al., 1994; Langer, 2000; Borden et al., 2002). Electrospinning, a technique that employs electric forces to produce polymer fibers with diameters ranging from 10 to 1000 nm, has gained significant attention due to its ability to fabricate structurally homogeneous nanofibers. However, traditional electrospun nanofibers often struggle to encapsulate bioactive agents at the nanoscale. Recent advancements, such as emulsion electrospinning, have enabled the production of composite nanofibers with nanoscaled drug particles embedded within biocompatible or biodegradable polymers, offering controlled drug encapsulation and release (Liao et al., 2008).

Emulsion electrospinning has been extensively investigated for creating nanofibrous drug delivery systems with core-shell structures, which are particularly effective for controlled and sustained drug release. Among the biodegradable polymers used in such systems, poly(lactic-co-glycolide) (PLGA) copolymers are widely recognized for their biocompatibility and tunable degradation properties. The degradation of PLGA, which involves bulk and surface erosion, is influenced by the ratio of lactide to glycolide in the copolymer. For instance, PLGA 50:50 degrades faster than PLGA 65:35 due to the higher hydrophilicity of glycolic acid, which accelerates polymer weight loss (Park, 1995; Makadia and Siegel, 2011). Similarly, PLGA 65:35 degrades more rapidly than PLGA 75:25 and PLGA 85:15. These variations in degradation rates allow for the tuning of drug release profiles, making PLGA a versatile material for drug delivery applications. Another notable biodegradable polymer, poly(ϵ -caprolactone) (PCL), has been widely explored in drug delivery and tissue engineering due to its tailorable properties. PCL offers a moderate drug release rate, longer degradation time, and lower adsorbable time compared to PLA or PLGA, making it suitable for applications requiring sustained release (Rai et al., 2016; Singh, 2012; Dash and Konkimalla, 2012).

Modeling the degradation and erosion of PLGA is essential for predicting drug release kinetics. Mechanistic approaches, such as those proposed in (Siepmann and Göpferich, 2001) and (Sackett and Narasimhan, 2011) are commonly employed to capture the complex interplay between polymer degradation, matrix porosity, and drug diffusion. These models account for changes in polymer molecular weight (MW) and porosity, which significantly influence drug release rates. For electrospun nanofiber mats, the hydrophobicity of the polymer matrix plays a critical role in drug diffusion. While hydrophilic macromolecular drugs are primarily limited to diffusion through pore spaces, smaller hydrophobic drugs can diffuse through both the polymer matrix and the pores, offering additional pathways for release (Zhu and Braatz, 2015).

Recent advancements in computational modeling have enabled the development of finite element models to simulate drug release from electrospun nanofibers. For instance, in (Kojic et

al., 2017) is introduced a radial finite element model to predict drug release kinetics from nanofibers. This approach has been further extended by (Milosevic et al., 2018, Milosevic et al., 2020) through the application of the KTM (Kojic transport model) and CSFE (composite smeared finite element) models, providing deeper insights into the mechanisms governing drug release from polymeric matrices. In the subsequent sections, we summarize our computational approach and provide an overview of the methodology used for modeling drug release from nanofibers.

2. Methodology

This section outlines the fundamental mathematical formulations governing diffusion and degradation processes. The modeling of mass release from fibers is carried out using 1D and composite smeared finite elements. The simulated environment includes both the fibrous structures and the adjacent medium, which is considered as a phenomenological fluid.

2.5 Detailed finite element model for drug release

A simple radial 1D finite element is used to model radial diffusion within fibers releasing drug to a surrounding medium which is represented using three-dimensional continuum FEs. The balance equation for diffusion follows the Fick's law. This radial 1D element provides reliable estimates of mass transport and proves to be computationally efficient for capturing diffusion behavior within the fiber and surrounding porous medium. Figure 1a presents a fibrous structure produced via a vertical electrospinning setup (CH-01, Linari Engineering, Pisa, Italy), conducted in the laboratory at the Faculty of Technology and Metallurgy, University of Belgrade. Based on imaging data, a three-dimensional fiber network is reconstructed, as depicted in Figure 1b, highlighting that drug diffusion proceeds both along the fiber and radial axis. While a full-scale finite element model could involve discretizing the entire domain—including fibers and interstitial pores—into 3D elements, such an approach would be computationally intensive and result in a vast system of equations. To circumvent these challenges, a radial 1D finite element model was developed following the methodology described by Kojic et al. (2017).

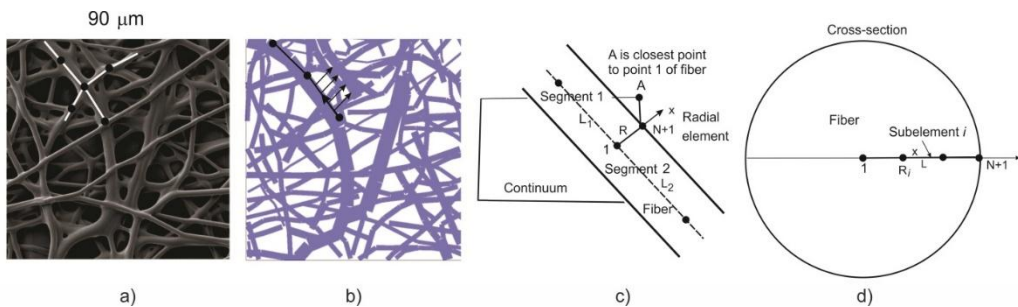


Fig. 1. a) Scanning electron microscopy (SEM) image showing the surface morphology of a PLGA fiber mat. b) Digitally reconstructed 3D fiber network used in the computational model, illustrating the directions of drug diffusion—both along the fiber axis and outward into the surrounding medium. c) Schematic representation of radial 1D finite elements distributed along the fiber length, with segments labeled L1 and L2 and a radial element positioned at node 1. d) Structure of a radial finite element subdivided into N smaller elements (Kojic et al., 2017).

The one-dimensional finite elements illustrated in Figures 1c and 1d are positioned along the fiber axis, corresponding to segment lengths denoted as L_1 and L_2 . Axial transport of the drug is simulated using standard diffusion modeling, where the governing equation incorporates nodal drug concentrations \mathbf{C}

$$\left(\frac{1}{\Delta t} \mathbf{M} + \mathbf{K}^{(i-1)} \right) \Delta \mathbf{C}^{(i)} = \frac{1}{\Delta t} \mathbf{M} (\mathbf{C}^{(i-1)} - \mathbf{C}^t) - \mathbf{K}^{(i-1)} \mathbf{C}^{(i-1)} \quad (1)$$

where details about matrices M_{1D} and K_{1D} all other details about radial diffusion from 1D elements are given in (Kojic et al., 2017, Milosevic et al., 2020, Kojic et al., 2022).

The influence of polymer degradation and matrix erosion on drug transport can be incorporated by adjusting the diffusion coefficient within the fiber structure. As proposed by (Zhu and Braatz, 2015), the effective diffusivity of the drug through PLGA polymer depends on the polymer's average molecular weight M_w and its internal porosity ϕ , i.e. $D_{fib} = D_{fib}(M_w, \phi)$.

This relationship $D_{fib}(M_w, \phi)$ can be mathematically described using the following equation:

$$D_{fib} = \frac{(1-\phi)D_s + \kappa\phi D_l}{1-\phi + \kappa\phi} \quad (2)$$

In this expression, D_s and D_l represent the diffusion coefficients within the solid polymer phase and the fluid-filled pores, respectively. The parameter κ denotes the partition coefficient, which characterizes the distribution tendency of the drug between the hydrophobic PLGA domain and the aqueous pore environment. Details about diffusivity D_s is given in (Zhu and Braatz, 2015).

Three-dimensional finite elements are employed to represent the space surrounding the fibers, and the governing mass balance is described by the balance equation provided in (Kojic et al., 2022).

$$\left(\frac{1}{\Delta t} \mathbf{M} + \mathbf{K}^{(i-1)} \right) \Delta \mathbf{C}^{(i)} = \mathbf{Q}^{S(i-1)} + \mathbf{Q}^{V(i)} - \mathbf{K}^{(i-1)} \mathbf{C}^{(i-1)} - \frac{1}{\Delta t} \mathbf{M} (\mathbf{C}^{(i-1)} - \mathbf{C}^t) \quad (3)$$

In this formulation, \mathbf{C} and \mathbf{C}^t denote the nodal concentration vectors at the current and previous time steps, respectively. The terms \mathbf{Q}^S and \mathbf{Q}^V correspond to flux contributions across the element surface and within its volume. The matrices \mathbf{M} and \mathbf{K} are given in (Kojic et al., 2022), where the diffusion coefficient D_{sur} is given in the diffusion matrix \mathbf{K} . The fiber-specific elements—both axial and radial—are derived from image-based geometries and integrated into the entire system using standard finite element assembly procedures. The predictive accuracy of the radial 1D finite element formulation was primarily validated through direct comparison with experimental drug release kinetics from fabricated PLGA implants, as reported in Milosevic et al., (2018). The close agreement between the computational results and empirical data established the model's reliability before its use as a benchmark for the developed smeared model. Boundary conditions and initial drug concentrations within the fibers are defined accordingly. Key structural parameters, including fiber diameter distribution, orientation, and the resulting volume fraction, were not assumed but were directly derived from the quantitative analysis of SEM images of the fabricated scaffolds, ensuring the model geometry accurately represented the physical system. The results obtained from this detailed model are later evaluated against the simplified smeared models presented in the next section.

2.6 Application of KTM in modeling drug release from nanofiber scaffold

The Composite Smeared Finite Element model incorporates both the volume fraction of fibers and their diameter distribution to simulate drug transport with improved fidelity. To enhance

model precision, a concept of correction functions is applied. The system is conceptually divided into two regions: the fibrous domain and the surrounding porous medium, characterized by volume fractions r_V and $(1 - r_V)$, respectively. Drug diffusion through the porous space is considered as a continuum process, governed by the mass balance equation described in Kojic et al. (2022)

$$\left(\frac{1}{\Delta t} \mathbf{M} + \mathbf{K}^v + \mathbf{K} \right)^{K(i-1)} \Delta \mathbf{C}^{K(i)} = \mathbf{Q}^{KS(i-1)} + \mathbf{Q}^{KV(i)} - \left(\frac{1}{\Delta t} \mathbf{M} + \mathbf{K}^v + \mathbf{K} \right)^{K(i-1)} \mathbf{C}^{K(i-1)} + \frac{1}{\Delta t} \mathbf{M}^K \mathbf{C}^{K(i)} \quad (4)$$

where \mathbf{K} represents fiber or pores (surrounding) domain. Axial diffusion along the fibers is reformulated into a continuum representation using a diffusion tensor, as outlined in (Kojic et al., 2017):

$$D_{ij} = \frac{1}{A_{tot}} \sum_K D_K \ell_{Ki} \ell_{Kj} \quad (5)$$

This transformation relies on fiber diameter data and directional cosines to capture anisotropic transport behavior. Furthermore, variations in the diffusion coefficient due to polymer degradation and erosion effects can be incorporated, as discussed earlier. Radial exchange of drug molecules between fibers and the adjacent pore space is modeled using 1D connectivity elements, following the approach in Kojic et al. (2022). To account for heterogeneities in the porous domain, a correction function introduced by Milosevic et al. (2020) is employed, along with an appropriate interpolation scheme.

3. User interface software for modeling diffusion from nanofibers

The user interface software CAD Field & Solid was utilized to execute the examples presented in this study. This software, which can be accessed and downloaded from the GitHub repository at <https://github.com/miljanmilos/CAD-Solid-Field>, is integrated with the PAK simulation code. It simplifies model generation and enables visualization and animation of computational results. As illustrated in Figure 2, the Example menu within the CAD software includes various modules. For modeling nanofibers, the Composite module offers two options: nanofibers for investigating drug transport using the detailed model, and nanofibers smeared for analyzing drug transport with the smeared (KTM) model.

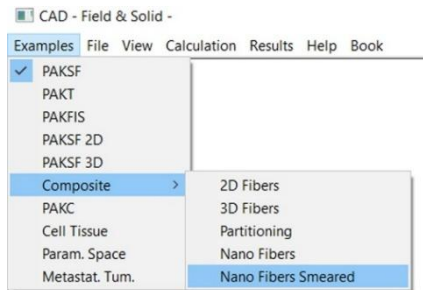


Fig. 2. a) Scanning electron microscopy (SEM) image showing the surface morphology of a PLGA fiber mat. b) Digitally reconstructed 3D fiber network used in the computational model, illustrating the directions of drug diffusion—both along the fiber axis and outward into the surrounding medium. c) Schematic representation of radial 1D finite elements distributed along the fiber length, with segments labeled L1 and L2 and a radial element positioned at node 1. d) Structure of a radial finite element subdivided into N smaller elements (Kojic et al., 2017).

To create a detailed model for the diffusion of RhB molecules from a PLGA implant, users can follow these steps: From the main menu, navigate to Book > Chapter 6 > Section 6.5 > Example 6.5.10a. The CAD software automatically reads the file \BookExamples\Ex_Book_Example6510a.txt and generates the model, as shown in Figure 3a. Parameters such as the size and density of the finite element (FE) mesh, as well as degradation properties, can be adjusted using the Nanofiber Implant Parameters dialog [16]. For the smeared model, users can select Book > Chapter 6 > Section 6.5 > Example 6.5.10b from the main menu. The CAD software reads the file \BookExamples\Ex_Book_Example6510b.txt and generates the model, as depicted in Figure 3b.

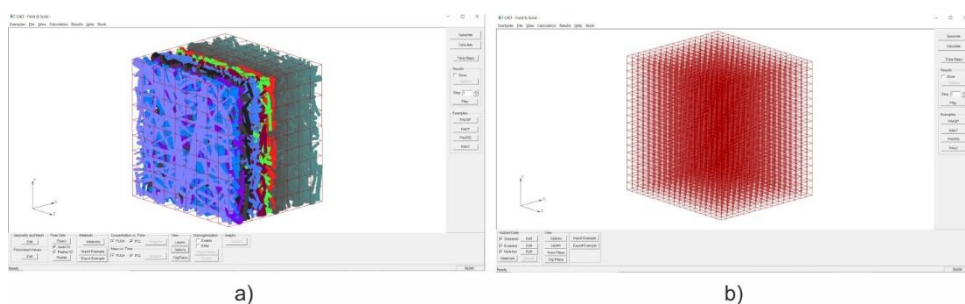


Fig. 3. a) CAD module NanoFibers for computational analysis of RhB mass release from a PLGA implant (detailed model), b) CAD module NanoFibers Smeared for computational analysis of RhB mass release from a PLGA implant (smeared model) (according to Kojic et al. 2022).

To generate a detailed model for the diffusion of RhB molecules from a three-layered PCL/PLGA/PCL fibrous scaffold, users can navigate to Book > Chapter 6 > Section 6.5 > Example 6.5.11a from the main menu. The CAD software automatically reads the file \BookExamples\Ex_Book_Example611a.txt, and clicking the Generate button produces the model displayed in Figure 4a. To incorporate the PCL layer, open the Nanofiber Implant Parameters dialog and select the Enable PCL Layer checkbox. This action activates the Edit boxes for LnPCL and NxPCL, allowing users to adjust the dimensions of the PCL layer and the mesh division in the longitudinal direction (Kojic et al., 2022).

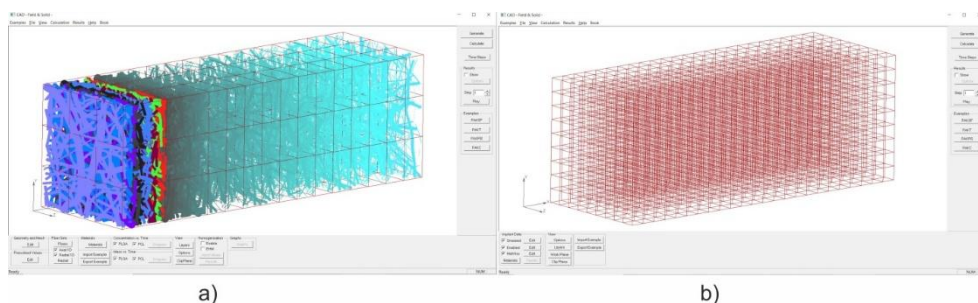


Fig. 4. a) CAD module NanoFibers for computational analysis of RhB mass release from a three-layered PCL/PLGA/PCL scaffold. b) A NanoFibers Smeared module within CAD for Example 6.5.11a, analyzing RhB mass release from a three-layered PCL/PLGA/PCL scaffold (according to Kojic et al., 2022).

To model the diffusion of RhB molecules from a three-layered PCL/PLGA/PCL scaffold using the smeared model, users can select Book > Chapter 6 > Section 6.5 > Example 6.5.11b from

the main menu. The CAD software reads the file \BookExamples\Ex_Book_Example6511b.txt and generates the model, as shown in Figure 4b. The Smeared Model Data dialog, similar to the one used in Figure 4b, allows users to adjust model parameters. Key adjustments include enabling the Enable PCL layer checkbox and defining parameters such as the length of the PCL layer (LnPCL), mesh division in the longitudinal direction (NxPCL), the volume fraction of fibers in the PCL layer (Rv), and the diffusion coefficient in the surrounding domain of the PCL layer.

4. Results

The following two examples illustrate the applicability of the computational models, according to (Milosevic et al., 2018, Milosevic et al., 2020).

4.8 Mass release of Rhodamine B (RhB) molecules from a PLGA implant

Two distinct PLGA-based nanofiber implants, labeled PLGA₁ and PLGA₂, were fabricated using the emulsion electrospinning technique. Subsequent drug release experiments were performed in the laboratories of the Faculty of Technology and Metallurgy, University of Belgrade. PLGA₁, with an average molecular weight (MW) of 40,000–75,000 g/mol, has a lactide-to-glycolide ratio of 65:35, while PLGA₂, with an MW of 30,000–60,000 g/mol, has a ratio of 50:50. Both implants measure 2.5 cm × 2.5 cm with a thickness of 160 μm. To simulate drug transport from PLGA₁ and PLGA₂ implants, two computational models were developed: (a) a detailed finite element (FE) model using 1D radial elements and (b) a composite smeared finite element (CSFE) model with two domains—fiber and surrounding domains. For the detailed FE model, the fiber network was reconstructed using in-house software based on an SEM image of drug-loaded PLGA fibers (90 μm × 90 μm), as shown in Figure 5a. By randomly duplicating and displacing the generated fiber layer along the longitudinal direction, a fiber mat representative of the implant was created (Figure 5b).

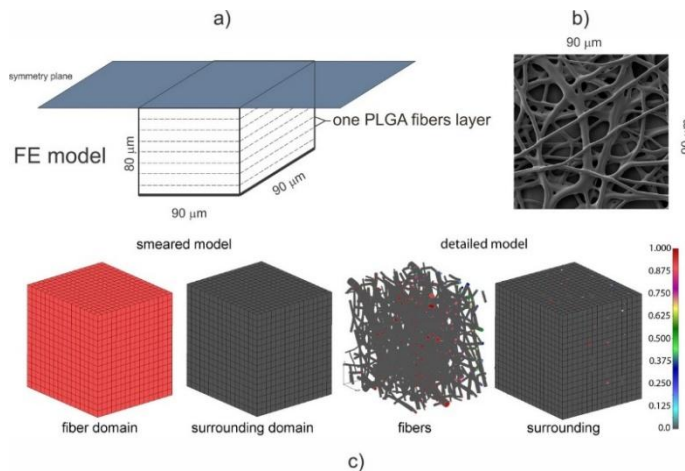


Fig. 5. FE model of the PLGA implant. a) The 3D modeling domain with a symmetry plane; b) SEM image of fibers c) FE model generated from an SEM image with accompanying concentration field for both smeared and detailed models and belonging domains (the PLGA domain is modeled using either a smeared composite finite element or a detailed fiber mesh) (according to Milosevic et al., 2018).

Assuming symmetry, only one half of the implant was modeled. Additionally, due to the homogeneous distribution of fibers, a small representative domain ($80\text{ }\mu\text{m} \times 90\text{ }\mu\text{m} \times 90\text{ }\mu\text{m}$) was used. The 3D FE mesh ($40 \times 48 \times 48$ divisions) comprised 64,512 nodes and 36,864 elements, with approximately 7,580 radial 1D elements. The CSFE model included two domains: the fiber domain (equivalent fiber representation) and the surrounding domain (equivalent pore space). Both the detailed and smeared models are illustrated in Figure 5 (bottom panel). The diffusion coefficient of Span 80/RhB in the pore space was assumed to be equal to that in water ($D_{\text{liquid}} = 0.04\text{ }\mu\text{m}^2/\text{s}$), while within the fibers, it was set to $D_{\text{fib}} = 4 \times 10^{-10}\text{ cm}^2/\text{s}$ (approximately 10^4 times lower than in water), based on (Ruiz-Esparza et al., 2014). The simulation spanned 75 days, divided into 15 time steps of 5 days each. The initial concentration in the fibers was set to $C_0 = 1$. Boundary conditions included no flux through model boundaries, except for $C = 0$ at the outer implant boundary, where mass release was measured. The mean fiber diameter was $D = 2.5\text{ }\mu\text{m}$.

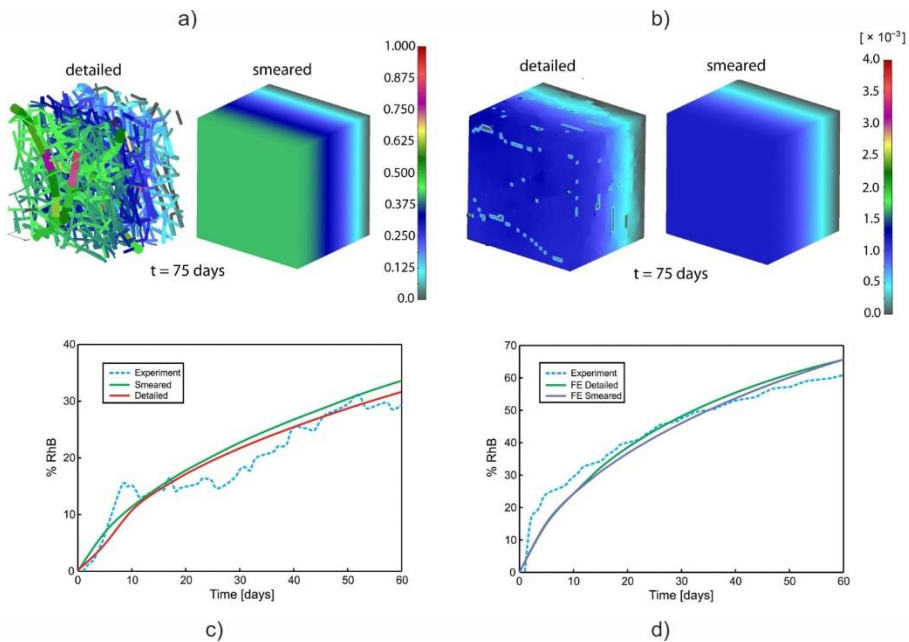


Fig. 6. PLGA implant—concentration fields in a) fibers and b) surrounding domains for detailed and smeared models, depicting Span-80/RhB complex diffusion. Cumulative release (%RhB) vs. time diagram for c) PLGA1 (65:35) and d) PLGA2 (50:50). A comparative analysis was performed between detailed models and their smeared counterparts, following the methodology outlined in Milosevic et al. (2018).

The concentration field within large vessels, liver tissue, and tumors is shown in Fig. 4a for three time points. It is noticeable that concentrations have the largest values in blood vessels (practically the same due to convection and large diffusion coefficient in fluid), following a decrease going to capillaries and tissue. Also, the concentration within tumor 2 is smaller compared to tumor 1 due to reduced diffusion coefficients. Evolution of the mean concentration within capillaries (capillary domain) and tissue of the liver, and tumors 1 and 2, is shown in Fig. 4b. The model gives insight into the transport of particles or molecules within the entire organ. In the first period, when the entering mass is increasing (entering concentration is increasing),

concentration within capillaries and tissue is increasing. The maximum concentration within capillaries has a delay with respect to the maximum of entering $c(t)$; and the maximums in tissue and tumors have further delays. Also, transport continues from capillaries to tissue as long as the concentration within capillaries is larger than in tissue. It is evident that concentration in tumor 1 is higher than in tumor 2 due to the larger diffusion and partitioning coefficients. This study demonstrates the effectiveness of both detailed and smeared models in accurately predicting drug release from PLGA nanofibers, validated by experimental data. The results highlight the potential of computational modeling to optimize drug delivery systems using electrospun nanofibers.

4.9 Drug release dynamics of Rhodamine B (RhB) from a multilayered PCL/PLGA/PCL fiber-based scaffold

The three-layered fibrous scaffold was produced through a stepwise electrospinning process conducted at the Faculty of Technology and Metallurgy, University of Belgrade. The first and third layers were composed of poly(ϵ -caprolactone) (PCL), while the middle layer was produced via emulsion electrospinning using poly(lactic-co-glycolic acid) (PLGA 65:35) impregnated with Rhodamine B (RhB). The complete scaffold measures $3\text{ cm} \times 4\text{ cm}$ with a total thickness of $560\text{ }\mu\text{m}$, comprising a $160\text{ }\mu\text{m}$ PLGA layer sandwiched between two $200\text{ }\mu\text{m}$ PCL layers. The morphology of the nanofiber mats was analyzed under conditions similar to those described in Figure 5, and the reconstructed fiber mesh served as input for a detailed finite element (FE) model utilizing 1D radial elements. A second model was developed using composite smeared finite elements (CSFE), which included two domains: the fiber domain and the surrounding domain.

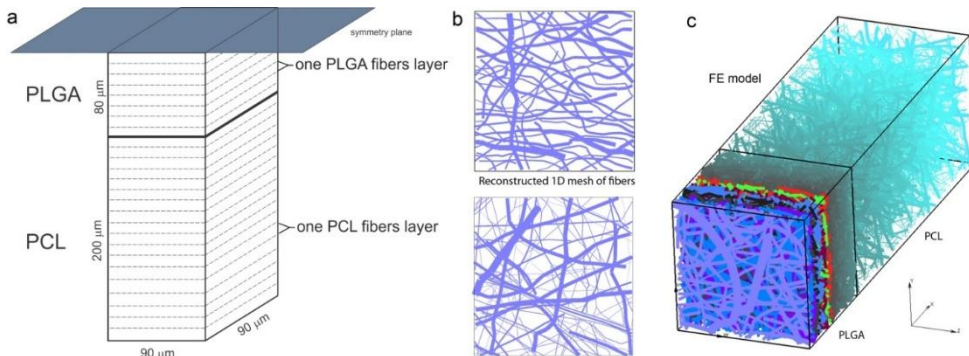


Fig. 7. a) Schematic layout of the finite element (FE) model representing the layered PCL/PLGA/PCL scaffold, including its geometric configuration. b) Digitally reconstructed one-dimensional mesh derived from mSEM images of individual PLGA and PCL fiber layers (scale bar: $20\text{ }\mu\text{m}$). c) Three-dimensional finite element representation of the trilayer scaffold, incorporating symmetry boundary conditions as described in Milosevic et al. (2020).

Based on the approach described by Milosevic et al. (2018), fiber mats for the PLGA and PCL layers were constructed by replicating and longitudinally shifting a base layer of one-dimensional fibers within the simulation domain, as illustrated in Figures 7b and 7c. The 3D FE mesh consisted of 70,785 nodes and 65,536 elements, with approximately 14,580 radial 1D elements. The surrounding domain in the PLGA layer incorporated "immersed" points to

account for the influence of fiber position and orientation on diffusion transport in the surrounding medium. A similar approach was applied to the PCL layer, assuming negligible diffusion through PCL fibers due to their slow degradation rate (approximately 6 months). The diffusion coefficient of RhB in the pore space (between fibers) was assumed to match that in water, while within the fibers (drug-impregnated), it was set to $D_{\text{fiber}} = 4 \times 10^{-10} \text{ cm}^2/\text{s}$. The simulation spanned 75 days, divided into 15 time steps of 5 days each. The initial RhB concentration in the PLGA fibers was uniform (C_0), and the outer scaffold boundary, where mass release was measured, was treated as an infinite reservoir with $C = 0$.

Within the smeared model, fiber-related transport was considered exclusively in the PLGA region, while the PCL layers were treated as passive, with no connection between the fiber domains of the PLGA and PCL layers. Drug transport was modeled as follows: RhB leaves the PLGA fiber domain, enters the surrounding PLGA domain, diffuses into the PCL surrounding domain, and finally exits the scaffold at the front boundary. Diffusion transport phenomena within the PCL fiber domain, as well as interactions between fibers and the surrounding medium via connectivity elements, were neglected in the model. Key parameters for the smeared model included: fiber volume fraction ($rV = 0.218$), mean fiber diameter ($5 \text{ }\mu\text{m}$, including a fiber distribution function), and diffusion coefficients ($D_{\text{wall}} = D_{\text{liquid}} = 0.04 \text{ }\mu\text{m}^2/\text{s}$). Degradation parameters matched those of the detailed model: partitioning coefficient ($P = 10^6$), degradation rate constants ($K = K_w = 2.5 \times 10^{-7}$, $\alpha = 1.714$), initial porosity (0), and diffusion coefficients ($D_{\text{plga}} = 0 \text{ }\mu\text{m}^2/\text{s}$, $D_{\text{liquid}} = 0.04 \text{ }\mu\text{m}^2/\text{s}$). The smeared FE model comprised 2,900 nodes and 2,268 elements, reducing the number of equations to be solved by approximately 20 times compared to the detailed model. Figure 8 presents the simulated concentration profiles for both the detailed and smeared models of the PCL/PLGA/PCL scaffold, depicting RhB diffusion within the fibers and surrounding domains over 75 days. The minimal differences between the two models confirm the accuracy and applicability of the smeared model for predicting drug transport in layered scaffolds.

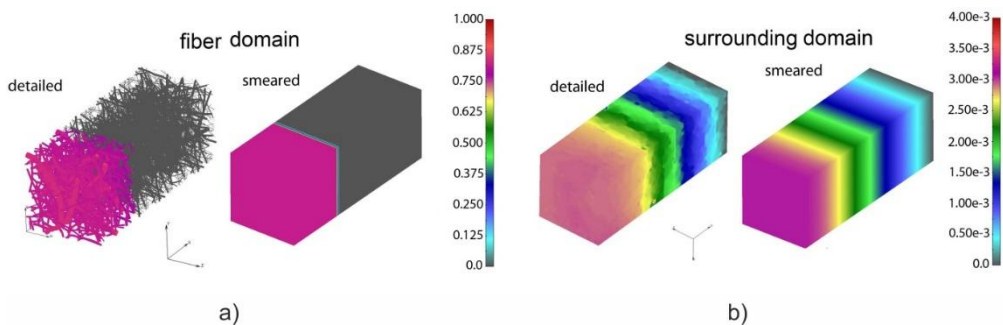


Fig. 8. a) Schematic layout of the finite element (FE) model representing the layered PCL/PLGA/PCL scaffold, including its geometric configuration. b) Digitally reconstructed one-dimensional mesh derived from mSEM images of individual PLGA and PCL fiber layers (scale bar: $20 \text{ }\mu\text{m}$). c) Three-dimensional finite element representation of the trilayer scaffold, incorporating symmetry boundary conditions as described in Milosevic et al. (2020).

A cumulative mass release diagram comparing experimental data and FE simulation results (detailed and smeared models) is presented in Figure 9. The close agreement between the models and experimental data demonstrates the reliability of the smeared model for predicting mass release in PCL/PLGA/PCL scaffolds.

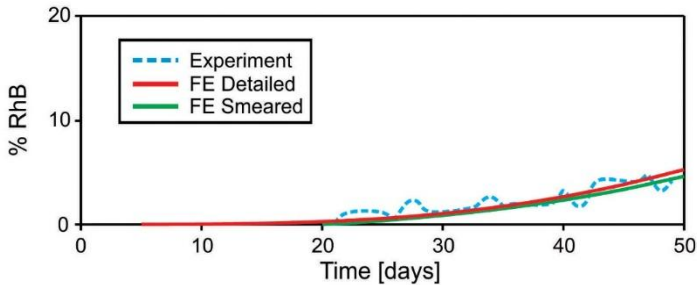


Fig. 9. Parameter-based prediction of the computational model. Cumulative release vs. time for RhB-impregnated 24 wt.% 65:35 PLGA. Experimental data (dashed line) and FE simulation results from detailed and smeared models (according to Milosevic et al., 2020).

The numerical FE model can be utilized to optimize scaffold design and predict mass release processes for various input parameters. Instead of conducting time-consuming experimental trials (often spanning months), the model provides a rapid and accurate means to predict drug release kinetics. Further details on parameter-based predictions and optimization are provided in (Milosevic et al., 2020).

5. Conclusion

This work provides an overview of numerical strategies based on the finite element method (FEM) for analyzing drug diffusion from nanofiber-based delivery systems. Two approaches—detailed and smeared models—were developed, incorporating partitioning and degradation effects, which are critical factors in drug delivery from nanofibers commonly used in implant design. Both models provide accurate predictions of drug release, with the detailed model utilizing radial 1D finite elements to represent drug transport. On the other hand, the smeared model utilizing CSFE for axial diffusion transport and connectivity elements for radial exchange, offers a computationally efficient and user-friendly alternative. The models were validated through experiments using electrospun PLGA nanofiber mats with varying compositions. Numerical results aligned well with experimental data, demonstrating the accuracy of both approaches in predicting diffusion processes. These models serve as effective tools for analyzing drug transport within polymer fiber networks and release into the surrounding porous medium. The combination of advanced fabrication techniques, such as emulsion electrospinning, with computational modeling provides a robust framework for designing next-generation drug delivery systems. Future research should focus on optimizing polymer compositions, exploring novel biodegradable materials, and refining predictive models to achieve precise control over drug release kinetics. Additionally, developing multifunctional nanofiber mats that integrate drug delivery with other therapeutic properties, such as

antimicrobial or anti-inflammatory effects, could further expand their applications in tissue engineering and regenerative medicine. In summary, electrospun nanofiber mats are a versatile and promising platform for controlled drug delivery. While demonstrated here for RhB in PLGA/PCL systems, the computational framework is general and can be applied to other drug-polymer combinations by measuring and inputting the relevant physicochemical parameters (e.g., drug diffusivity, partition coefficient, polymer degradation rate) into the model. By leveraging advancements in polymer science, fabrication techniques, and computational modeling, researchers can design tailored drug delivery systems to address the specific needs of diverse therapeutic applications.

This paper represents a summary of our research in this field in the last few years and is devoted to the celebration of 50 years of the development and application of the FE software PAK.

Acknowledgements: This work was supported by the Ministry of Science, Technological development and Innovation of Serbia (contract number 451-03-136/2025-03/200378), and by the City of Kragujevac, Serbia.

References

- Borden, M., Attawia, M., Laurencin, C.T., 2002. The sintered microsphere matrix for bone tissue engineering: in vitro osteoconductivity studies. *J. Biomed. Mater. Res.*, 61, 421–42. Liao, Y.
- Dash, T. K., Konkimalla, V.B., 2012. Poly- ϵ -caprolactone based formulations for drug delivery and tissue engineering: A review. *J. Con. Release*, 158(1), 15-33, 10.1016/j.jconrel.2011.09.064.
- Kojic, M., Milosevic, M., Simic, V., Stojanovic, D., Uskokovic, P., 2017. A radial 1D Finite Element for Drug Release from Drug Loaded Nanofibers, *J. Serb. Soc. Comp. Mech.*, 11, 1, 82-93.
- Kojic M, Milosevic M, Ziemys A, *Computational Models in Biomedical Engineering - Finite Element Models Based on Smeared Physical Fields: Theory, Solutions, and Software*, 1st Edition, Elsevier, September 11, 2022, ISBN: 9780323884723.
- Langer, R., 2000. Biomaterials in drug delivery and tissue engineering: one laboratory's experience. *Acc. Chem. Res.*, 33, 94–10.
- Makadia, H.K., Siegel, S.J., 2011. Poly Lactic-co-glycolic acid (PLGA) as biodegradable controlled drug delivery carrier. *Polymers*, 3, 1377–1397.
- Milosevic, M., Stojanovic, D., Simic, V., Milicevic, B., Radisavljevic, A., Uskokovic, P., Kojic, M., 2018b. A Computational Model for Drug Release from PLGA Implant, *Materials*, 11(12), 2416; <https://doi.org/10.3390/ma11122416>.
- Milosevic, M., Stojanovic, D. B., Simic, V., Grkovic, M., Bjelovic, M.P., Uskokovic, S., M. Kojic, 2020. Preparation and modeling of three-layered PCL/PLGA/PCL fibrous scaffolds for prolonged drug release, *Scientific Reports*, <https://doi.org/10.1038/s41598-020-68117-9>.
- Park, T.G., Alonso, M.J., Langer, R., 1994. Controlled release of proteins from poly (l-lactic acid) coated polyisobutylcyanoacrylate microcapsules. *J. Appl. Polym. Sci.*, 52, 1797–1807.
- Park, T.G. Degradation of poly(lactic- co-glycolic acid) microspheres: Effect of copolymer composition. *Biomaterials* 1995, 16, 1123–1130.

- Rai, A., Senapati, S., Saraf, S. K., Maiti, P., 2016. Biodegradable poly(ϵ -caprolactone) as a controlled drug delivery vehicle of vancomycin for the treatment of MRSA infection, *J. Mater. Chem. B*, 4, 5151–5160; 10.1039/C6TB01623E.
- Ruiz-Esparza, G. U. et al. Polymer nanoparticles enhanced in a cyclodextrin complex shell for potential site- and sequence-specific drug release. *Adv. Funct. Mater.* 24, 4753–4761. <https://doi.org/10.1002/adfm.201400011> (2014).
- Sackett, C.K., Narasimhan, B., 2011. Mathematical modeling of polymer erosion: Consequences for drug delivery. *Int. J. Pharm.*, 418, 104–114.
- Singh, N. K., 2012. Nanostructure controlled anti-cancer drug delivery using poly(ϵ -aprolactone) based nanohybrids, *J. Mater. Chem.*, 22, 17853–17863; 10.1039/C2JM32340K.
- Siepmann, J., Geopferich, A. 2001. Mathematical modeling of bioerodible, polymeric drug delivery systems. *Adv. Drug Deliv. Rev.*, 48, 229–247.
- Zhu, X., Braatz, R.D., 2015. A mechanistic model for drug release in PLGA biodegradable stent coatings coupled with polymer degradation and erosion, *J. Biomed. Mater. Res. Part A*, 103, 2269–2279.
- Zhang, L., Gao, Y., Zhu, Z. T. & Fong, H. Preparation, characterization, and encapsulation/release studies of a composite nanofiber mat electrospun from an emulsion containing poly (lactic-co-glycolic acid). *Polymer* 49(24), 5294–5299. <https://doi.org/10.1016/j.polymer.2008.09.045> (2008).